Powder Technology 384 (2021) 267–275

Contents lists available at ScienceDirect

Powder Technology

journal homepage: www.elsevier.com/locate/powtec

Comparison of surface energy and adhesion energy of surface-treated particles

Bernardo Moreno Baqueiro Sansao [a,*], Jon J. Kellar [a,b], William M. Cross [a,b], Karen Schottler [b], Albert Romkes [c]

[a] Materials Engineering and Science Graduate Program, South Dakota School of Mines and Technology, Rapid City, SD, United States of America
[b] Department of Materials and Metallurgical Engineering, South Dakota School of Mines and Technology, Rapid City, SD, United States of America
[c] Department of Mechanical Engineering, South Dakota School of Mines and Technology, Rapid City, SD, United States of America

ARTICLE INFO

Article history:
Received 21 February 2020
Received in revised form 3 December 2020
Accepted 13 February 2021
Available online 19 February 2021

Keywords:
Surface energy
Adhesion
Dry processing
Sustainability

ABSTRACT

The mineral industry uses tremendous amounts of water every year in the processing of ores. Sustainable practices associated with the processing of ores are, therefore, of critical importance. The project described herein is the first step toward producing a dry, particle-separation process based upon control and exploitation of adhesive forces. In this research, the goal is to determine the surface energy of particles, and further, whether the solid surface energy can be used to understand the adhesion between these particles and surface-modified substrates. Glass spheres were chosen to represent silicate minerals, the most abundant type of minerals found in mineral deposits. The solid surface energy was found by using contact angle measurements and by applying the van Oss-Good-Chaudhury (VOGC) method. The VOGC method utilizes three-liquid triads to determine the Lifshitz-van der Waals, Lewis acid and Lewis base surface energy components. Surface energies from plasma-cleaned glass were between 40.2 and 60.2 mJ/m^2; for the same glass with a hydrophobic chemical surface treatment, trichloro(octadecyl)silane (TCOD), the surface energy was between 20.8 and 20.9 mJ/m^2; and for the glass with a hydrophilic chemical surface treatment (n[1]-(3-trimethoxysilylpropyl) diethylenetriamine (TMPA)) the surface energy was between 46.3 and 61.6 mJ/m^2. The particle-substrate adhesion was also measured using a mechanical impact tester. Glass disks and beads were used, cleaned and surface treated with TCOD and TMPA. A custom horizontal impact tester was designed and used to measure the adhesion force between the glass spheres and a glass disk substrate. Impact of the disk/particle puck causes particle removal as tensile forces act on the particles. The tensile detachment force and adhesive force are equal at a critical particle size. Johnson-Kendall-Roberts (JKR) theory was used to determine the interfacial energy between the particles and the surface. The average interfacial energy of plasma cleaned glass, glass treated with TCOD and with TMPA were 44.8 mJ/m^2, 21.6 mJ/m^2, and 40.1 mJ/m^2, respectively. These values are in good agreement with the literature values and with the interfacial energy determined using the VOGC method described above, demonstrating that two approaches compare favorably, despite the dramatically different methods (molecular vs mechanical) utilized.

1. Introduction

The mineral industry requires tremendous amounts of water to separate valuable minerals from ores. A common process to separate minerals is froth flotation which is commonly conducted between 25 and 40 wt% solids [1]. The requirement of water in a conventional comminution-classification-flotation circuit to process, for instance, copper sulfide ore, is approximately 1.5 to 3.5 m^3 of water per metric ton of ore processed [2]. In addition, most of the copper mines in the United States are located in the arid desert southwest (e.g. Arizona and New Mexico). Thus, sustainable processing, using reduced water consumption is of critical importance to the long-term viability of such operations.

Over the past 10–15 years significant progress has been made with dry air-based separation systems. Probably the most widely adopted systems are so called sensor-based sorter systems [3]. There have been significant advancements in this technology, largely because of improved imaging, sensing and separation algorithms. The sorter systems typically transport a dry feed (particle size 2–50 mm) on a conveyer belt over the sensing area. The sensing technology used depends upon the feed material and the desired separation. In particular, sorter technology has found utilization with separation of plastics and gemstones. The separator uses sensors that can detect and sort (via an air blast) by particle chemistry, and similarly, the particles can be sorted based upon color/spectral response. Mineral sensing separations have

* Corresponding author at: South Dakota School of Mines and Technology, Department of Materials and Metallurgical Engineering, 501 East Saint Joseph Street, Rapid City, SD 57701, United States of America.
E-mail address: bernardo.sansao@mines.sdsmt.edu (B. Moreno Baqueiro Sansao).

https://doi.org/10.1016/j.powtec.2021.02.029
0032-5910/

lagged, in use, behind other applications (e.g. plastics), and are usually practiced for relatively high-grade mineral streams that liberate at a large particle size. In other words, sorter systems currently are not amenable for low grade ores that often need to be ground to less than 200 μm (an order of magnitude smaller than used with sensor-based sorter systems) to achieve acceptable liberation.

In addition to sorting technologies, air tables, air jigs and air-dense medium are other types of dry air-based separators. These can all be considered dry-based advanced sorting technologies, and in particular the magnetic air dense medium technology (MADMT) has drawn significant interest for separating inorganic ash from coal [4–8]. The MADMT separating device is a fluidized bed that includes very finely ground magnetic powders. At intermediate bed density (between the lower density coal and higher density inorganic minerals) separation is achieved by suspending the magnetic particles. The coal then levitates to the top of the fluidized bed and the inorganic minerals to the bottom. These systems suffer from the need to add an external magnetic medium, are dynamically unstable, and work best on systems that have large differences in densities and large size of particle liberation (~10 mm). These constraints have limited application almost exclusively to coal/mineral separations.

Exploitation of differences in adhesive forces between particles and a flat substrate is one additional potential gateway to develop a dry, sustainable process for mineral separation and concentration. Measurements of adhesive forces can be accomplished through various techniques [9–11] and are often somewhat tedious and time consuming. Regardless of these challenges, it is important to understand how the surface energy of solids contributes to the adhesion of particles to a substrate, and this was the focus of this research.

A solid's surface energy can be thought of as the amount of energy required when molecular bonds are broken to form a new solid's surface [12,13]. With regard to interfacial adhesion, there are several sets of forces in operation across the interface. One set is the van der Waals forces, which include London dispersion forces between induced dipoles (all surfaces exhibit these forces); Debye forces, between a permanent dipole and an induced dipole (polar to non-polar); and Keesom forces, between permanent dipoles (polar to polar). The other force is the electron accepting/donating behavior of Lewis acid/base pairs. Combined, these forces attract (or repel) material within a molecular proximity to a solid surface. However, if a surface is treated such that it has low polarity, particles will not have strong adherence because only weak, non-polar (London) van der Waals forces bond the materials. If there is other interference/contamination on the surface, like dirt, oils or residue from the atmosphere, the Lewis acid, base and Lifshitz-van der Waals sites could be covered and replaced with low energy material, keeping the desired material from attaching. This research compares surface energies of glass in its natural state and treated with hydrophobic coatings, which would have few polar groups, and hydrophilic coatings, whose surfaces will have significant numbers of polar groups. Furthermore, the higher the surface energy of a mineral, the more materials of high surface energy will adhere to the mineral's surface [13].

A variety of methods for calculating the surface free energy of solids using the contact angle a liquid makes with a solid surface are usable, which generally yield similar values for the solid surface energy [14,15]. In this research this is referred to as a *'molecular approach'* to measuring surface free energy. The van Oss-Good-Chaudhury acid-base method (VOGC) which includes the Lifshitz-van der Waals, Lewis acid and Lewis base interactions between solid and liquid [14–17] has been used in this work. The VOGC method uses a triad of three liquids with known surface tension components. Triads are chosen to minimize their condition number to yield accurate surface energy values [14]. To find the Lifshitz-van der Waals component, a non-polar liquid is used (e.g. diiodomethane (CH_2I_2)). Also needed are a liquid that is heavily dominant Lewis acid (e.g. water) and one that is highly Lewis basic (e.g. ethylene glycol ($C_2H_6O_2$) or glycerol ($C_3H_8O_3$)). There has been some debate in the literature with the scales used [18] but these issues are related to inter-comparison of the components, not with the measured total solid surface energy. The surface energy can be used to determine the adhesion between two solids [10]. The most accurate calculation of surface energy comes from using the advancing angle of the contact angle hysteresis (the difference between the advancing angle and the receding angle) [19]. When the surface with the adhering drop is tilted, advancing (down-hill) and receding (up-hill) angles form. The advancing angle is the angle measured just before the liquid begins to slide and is the instance of strongest adhesion for that solid [19]. Thus, using the advancing angles in the VOGC method yields solid surface energy values that represent the lowest energy regions of the surface [15].

In 1971 Johnson, Kendall and Roberts (JKR) developed a model that includes the effect of adhesion force on the deformation of an elastic sphere in contact with an elastic half space [20]. As previously stated by Zafar et al. [9] the JKR theory is an adhesion energy theory that infers that "the pressure distribution at contact is such that all short-range contact forces exist within the contact area" adding an adhesion force to the classical Hertz [21] contact theory. However, when using a solid with high elastic modulus (glass in this case), the deformation produced by the attractive forces is very small [20], thus the deformations can be neglected. Zafar et al. [9] utilized JKR theory to develop a drop test method for the determination of particle adhesion (interfacial energy). In this research the Zafar method was adapted to measure interfacial energy in what is referred to here as a *'mechanical approach'*.

Researchers have previously examined the correlation between surface energy and adhesion, particularly in polymer and polymer matrix composite samples [10,11,22–24]. In addition, mineral surface energy components have been correlated with mineral separation response [25,26]. In the polymer and composite studies, a strong correlation between surface energy and mechanical adhesion was often observed, although some deviation was noted, possibly related to roughness of the surface altering the contact area. With respect to mineral separation, a direct correlation between the work of adhesion and separation has been observed [25,26].

The optimal condition in this is work is to have comparable results of measured interfacial energy using a quick test (mechanical approach) with the VOGC method to calculate the surface energy (molecular approach).The specific property compared here is the surface and interfacial energy of glass under different chemical treatments. The surface and interfacial energy are compared using two different methods: a molecular and a mechanical approach. The obtained data was compared to literature results. The benefits of treating a surface with a chemical is to change its surface energy and be able to apply this in a system to separate particles of different surface energies.

2. Materials and methods

For the measurement of contact angle between the liquids elected for this investigation, and the glass slides, a Ramé-Hart Model 500 Goniometer/Tensiometer was used. The selected probe liquids for the series of tests were: distilled water (H_2O, noted as W), ethylene glycol ($C_2H_6O_2$, noted as E), glycerol ($C_3H_8O_3$, noted as G), diiodomethane (CH_2I_2, noted as D), and dimethyl sulfoxide (C_2H_6OS, noted as S). We chose diiodomethane, because it is the nonpolar liquid with the greatest surface tension. Water was chosen for its cost, ubiquity, high surface tension and primarily that it is one of the few liquids that has a high acidic component. The other three liquids are common liquids that are often used as the basic portion of the VOCG triad. Each liquid's contact angle was measured on separate disks and with each drop either 5 or 10 μl in volume. Each angle was measured 45 times per drop, and the resulting angle used was the average of the left side of the drop. The advancing angles for each substrate and set of liquids were measured using the automatic tilting function of the goniometer. The down-hill side of contact angle hysteresis is the point where the surface adhesion is strongest. This angle can give a more realistic value for the surface free

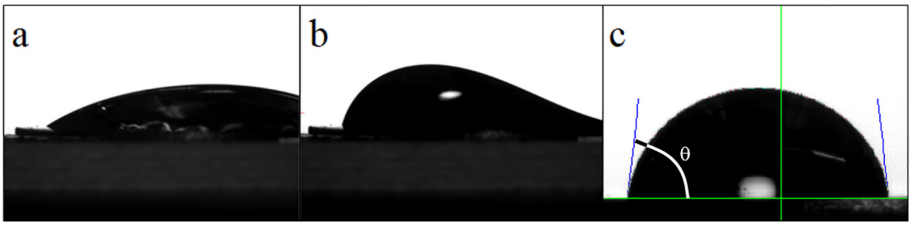

Fig. 1. (a) sessile drop, (b) advancing drop and (c) measurement of the contact angle (θ) of a sessile drop made by the equipment (the inner angle between the drop and the surface).

energy than the angles measured from a sessile drop on a level surface. Fig. 1 shows a sessile drop and an advancing drop of a 10 μl volume of water over a glass disk.

Glass disks of 8 mm in diameter, purchased from Electron Microscopy Sciences, were tested with three different surface treatments, specifically, i) plasma cleaned using a Harrick Plasma Cleaner, where the disks were treated for at least 5 min on each side; ii) treated with trichloro(octadecyl)silane (TCOD) after plasma cleaning; and, iii) treated with n^1-(3-trimethoxysilylpropyl) diethylenetriamine (TMPA) after plasma cleaning. See Fig. 2 for the structure of these molecules. Both chemicals were supplied by Sigma-Aldrich®.

The treatment with TCOD was performed in a solution of 1.5 ml of this substance and 40 ml of toluene for each 2 g of glass used. Beads and disks were treated in different containers. The glass particles were agitated in solution for 2 h and then cured (dried) for 2 h at 150 °C.

TMPA was used as a 5% *v*/v solution in absolute methanol, with 100 ml of solution for every 4 g of glass prepared. The same solution contact time and curing time were applied in this treatment as was used in the hydrophobic treatment.

Using the van Oss-Good-Chaudhury method, at least three liquids are necessary to calculate the solid surface energy components. Eqs. (1–3) show how the surface energy is calculated, while Eq. (4) shows the calculation of the thermodynamic work of adhesion. Basically, the thermodynamic work of adhesion is equated to the sum of the geometric mean of the interacting components. The Lifshitz-van der Waals (LW) components interact, while acid (a) components interact with base (b) components [27].

$$\gamma_{L_1G}(1+\cos\theta_1) = 2\left(\gamma_{L_1G}^{LW}\gamma_{SG}^{LW}\right)^{0.5} + 2\left(\gamma_{L_1G}^{a}\gamma_{SG}^{b}\right)^{0.5} + 2\left(\gamma_{L_1G}^{b}\gamma_{SG}^{a}\right)^{0.5} \quad (1)$$

$$\gamma_{L_2G}(1+\cos\theta_2) = 2\left(\gamma_{L_2G}^{LW}\gamma_{SG}^{LW}\right)^{0.5} + 2\left(\gamma_{L_2G}^{a}\gamma_{SG}^{b}\right)^{0.5} + 2\left(\gamma_{L_2G}^{b}\gamma_{SG}^{a}\right)^{0.5} \quad (2)$$

$$\gamma_{L_3G}(1+\cos\theta_3) = 2\left(\gamma_{L_3G}^{LW}\gamma_{SG}^{LW}\right)^{0.5} + 2\left(\gamma_{L_3G}^{a}\gamma_{SG}^{b}\right)^{0.5} + 2\left(\gamma_{L_3G}^{b}\gamma_{SG}^{a}\right)^{0.5} \quad (3)$$

$$W_{adh} = 2\left(\sqrt{\gamma_{disk}^{LW} * \gamma_{bead}^{LW}}\right) + 2\left(\sqrt{\gamma_{bead}^{a}\gamma_{disk}^{b}} + \sqrt{\gamma_{disk}^{a}\gamma_{bead}^{b}}\right) \quad (4)$$

Where γ is the surface free energy (mJ/m^2), L_iG is the liquid-gas component, *SG* is the solid-gas component, *LW* indicates the Lifshitz-van der Waals component (mJ/m^2), *a* indicates the Lewis acid component (mJ/m^2), *b* indicates the Lewis base component (mJ/m^2), θ_i is the contact angle between the liquid and the solid (in degrees), bead indicates the glass bead, disk indicates the glassdisk. By knowing the *LW*, *a* and *b* components of each of the liquids and measuring the contact angle between the liquid and the substrate, each γ_{SG} component can be calculated by solving Eqs. (1–3) simultaneously. Eq. (4) indicates that for a bead and a disk with the same surface treatment that the work of adhesion (W_{adh}) should be between one and two times the determined solid surface energy.

For the determination of particle adhesion, the interfacial energy was determined based on an impact test first developed by Zafar et al. [9], and adapted for the needs of this research. In this investigation, micron size glass spheres (size range between 10 and 100 μm and density of 2.48 g/cm^3) were chosen to represent silicate minerals, the most abundant type of mineral found in mineral deposits [28], and to work as model particles. Fig. 3 shows the scanning electron micrograph (SEM) of the beads tested. The glass beads were purchased from PolyScience. The substrates where the particles are attached are the same glass disks used in the contact angle experiments described earlier. The beads were also plasma cleaned (for 10 min) and treated with TCOD and TMPA following the same procedures detailed previously.

Glass disks were glued to an aluminum stub of about 15 mm in diameter and 25 mm in length. The beads were then sprinkled over the disk, yielding a single layer of beads covering most of the disk area; an example of this is shown in Fig. 4. In order to measure the interfacial velocity, a portable device was designed and fabricated. A horizontal tube with maximum length of 50 cm, was mounted on an aluminum base supported by aluminum columns (providing enough weight to hold the system in place during the tests). An aluminum backstop with an opening of 12 mm was placed at the end of the glass tube. The aluminum stub was then propelled using an air compressor with a pressure regulator, adjusting the pressure to achieve the desired velocity. The stub accelerated and impacted on the backstop against the opening at the end of the tube. The velocity and duration of impact were measured using a high-speed camera (IDT MotionProY Series 4), recording every

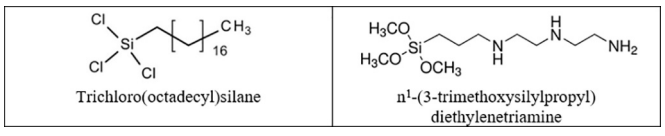

Fig. 2. Structures of TCOD and TMPA.

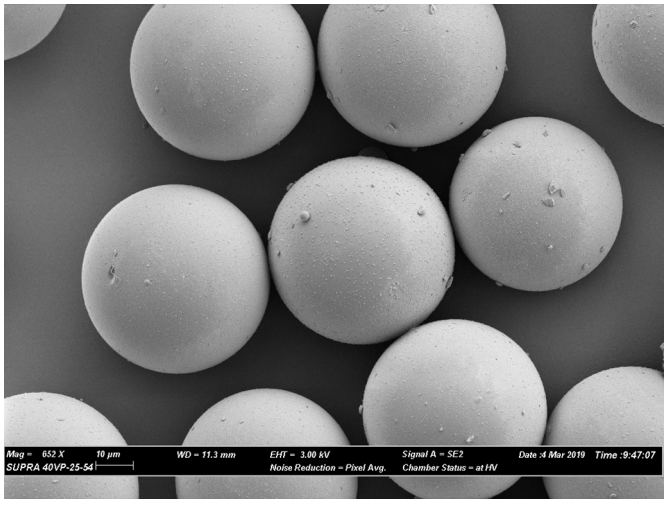

Fig. 3. SEM micrograph of glass beads.

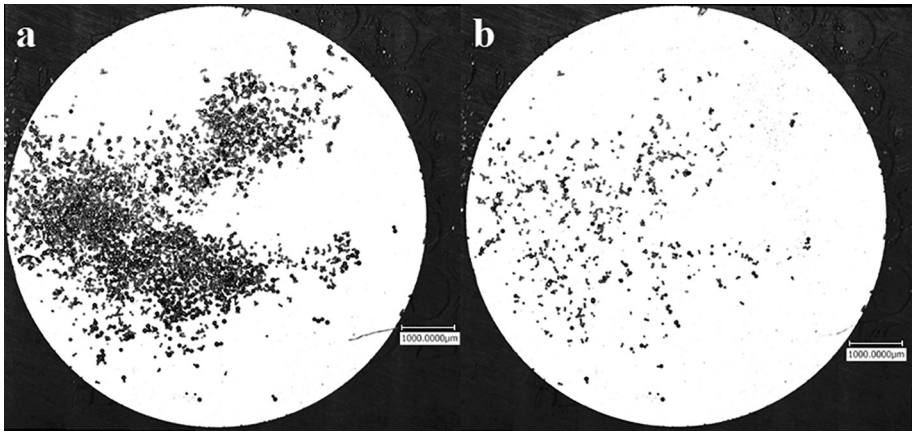

Fig. 4. Plasma-cleaned glass disk with glass beads a) before and b) after impact.

impact at a rate of 70,000 frames per second. The impact provoked a tensile force between particle and surface because of the sudden stub deceleration. The Supplementary Material contains a schematic representation of the impact test system in Fig. S1. (A video of an example of the impact can be seen at https://youtu.be/KZeUVPA-pxg).

The adhesion force between two bodies is obtained by following the same application of JKR theory used by Zafar et al. [9], which uses Eq. (5), where F_{ad} is the JKR [20] adhesive force, Γ is the interface energy and R is the particle radius. The detachment force of a particle due to momentum is obtained from Eq. (6), where F_{det} is the detachment force, *m* is the mass of the particle, Δt is half of the time of impact (i.e. half of the time of contact between stub and backstop) and *v* is the impact velocity. The interface energy was then estimated from Eq. (7), where $F_{det} = F_{ad}$.

$$F_{ad} = \frac{3}{2}\pi R\Gamma \tag{5}$$

$$F_{det} = \frac{m\Delta v}{\Delta t} \tag{6}$$

$$\Gamma = \frac{m\Delta v}{\Delta t \pi R}\frac{2}{3} \tag{7}$$

Whenever the adhesive force is greater than the detachment force ($F_{ad} > F_{det}$), particles will remain attached on the disk surface for a given particle size. There is a critical particle size at which $F_{ad} = F_{det}$. This critical size indicates that particles will detach if they are bigger than the critical size and particles will remain attached if they are smaller than the critical size [9]. An image of the beads on the surface of the disk was taken before (see Fig. 4a) and after (see Fig. 4b) each test using a laser profilometer (Keyence VK 200×). The image of the disk after the test was then analyzed using ImageJ software to determine the size of the beads that remain attached to the disk. The largest size left on the disk was used to calculate the adhesion energy of the particles.

3. Results and discussion

Disks treated with TMPA and TCOD were placed in capped vials for two hours, 24 h and 36 h. Figs. 5 and 6 show the results of the contact angles measured with different liquids. As the TMPA is hydrophilic and having a high surface energy, the treatment was less stable over time compared to the TCOD treatment, and hence all contact angle measurements were conducted in a timely manner (within the day of treatment). The contact angle with water showed a variation from 48.6 degrees (in 2 h) to 34.2 degrees (after 36 h). The TCOD being hydrophobic and having a low surface energy did not show any significant

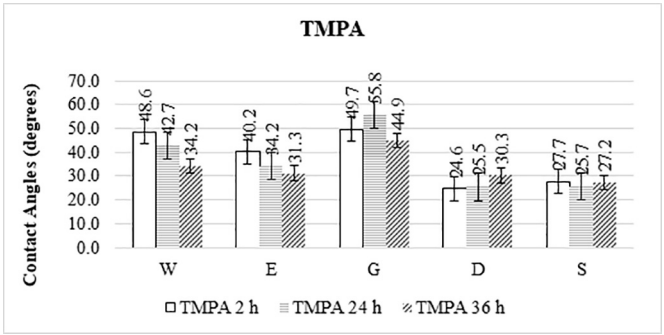

Fig. 5. Comparison of 2-h, 24-h, 36-h old TMPA treatment on glass.

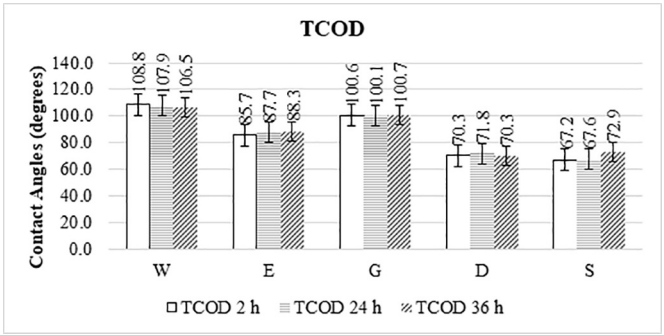

Fig. 6. Comparison of 2-h, 24-h, 36-h old TCOD treatment on glass.

variation. Regardless of coating, the disks were cleaned and treated and tested within the same day.

Sessile drop contact angles and advancing and receding contact angles for glass disks coated with TMPA are shown in Fig. 7 and with TCOD in Fig. 8. The same drop of liquid was used for the sessile drop, the advancing and the receding measurement. The sessile angle was measured first before tilting the goniometer and then measured again for the advancing/receding angle. The advancing angles for both TMPA and TCOD are higher than the sessile angles, which means the advancing angles will produce a lower value for surface energy for that solid; consequently, the receding angles are smaller than the sessile angles, which means the receding angles will produce a higher value for surface energy for that solid. The TMPA treatment showed higher variation from the sessile drop contact angle to the advancing contact angle when comparing the two different measurements with the TCOD treatment.

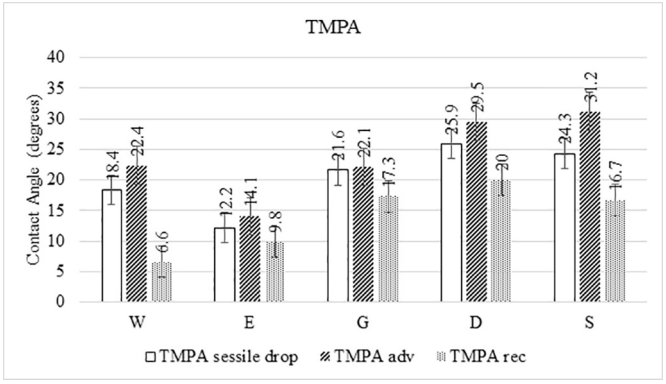

Fig. 7. Comparison of advancing (TMPA Adv), receding (TMPA rec) and sessile (TMPA sessile drop) contact angles for the five probe liquids tested on TMPA treated glass.

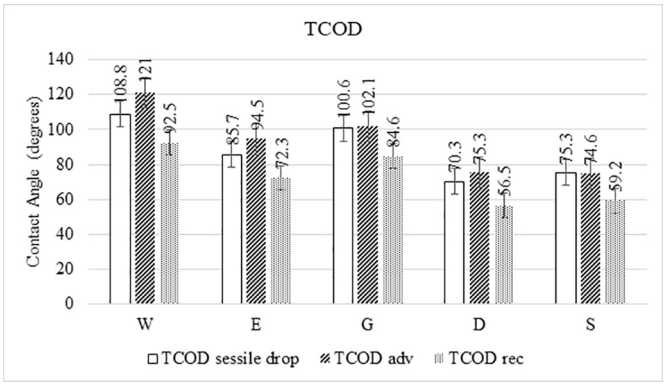

Fig. 8. Comparison of advanced (TCOD Adv), receding (TCOD rec) and sessile (TCOD sessile drop) contact angles for the five probe liquids tested on TCOD treated glass.

Table 1 shows the experimental results for the Lifshitz-van der Waals (*LW*) components, acid components (*a*) and base components (*b*) for each glass treatment using Eqs. (1–3). Table 2 lists the surface free energy for the substrates tested during this investigation. The liquids triads shown in Table 2 were chosen due to their well-balanced nature which leads to low condition numbers and, hence, more accurate solutions to the VOGC equations. To achieve these low condition number solutions, typically, one chooses a dispersive liquid (dioodomethane, D), a more acidic liquid (water, W), and a more basic liquid (ethylene glycol, E, glycerol, G, and dimethyl sulfoxide, S). The condition numbers for theses triads are 6.28 for W-D-E, 8.11 for W-D-G, and 7.19 for W-D-S. The condition number was calculated considering only the surface energy components of the probe liquids [29]. A table with the calculated condition numbers of the possible triads from the five probe liquids used is show in Table T1 in the supplementary material. The surface energy value is a result by solving Eqs. (1–3) simultaneously. The surface energy values calculated by the VOCG method for treated glass in this work were compared to calculations using a different approach. The different approach chosen was that of Chibowski and Perea-Carpio (CPC method) [30]. The CPC method uses the cosine of the advancing and receding contact angle to calculate the total solid surface energy. For TMPA-treated glass surfaces with contact angle data presented in Fig. 7, the solid surface energy calculated was 52.7 mJ/m^2, which is close to the sessile drop and advancing contact angle vOGC calculations of 55.9 and 54.8 mJ/m^2; the vOCG receding contact angle surface energy was considerably greater than the CPC method value; for the TCOD-treated glass surfaces with contact angle data presented in Fig. 8, the solid surface energy calculated was 21.9 mJ/m^2, which is very close to the sessile drop and advancing contact angle VOCG calculations of 22.5 and 20.9 mJ/m^2; the VOCG receding contact angle surface energy was considerably greater than the CPC method value.

Table 1
Experimental Lifshitz-van der Waals (LW) components, acid components (a) and base components (b) calculated for each glass treatment with the sessile drop method – in mJ/m^2.

Material	*LW*	*a*	*b*
Plasma Cleaned Glass	43.48	0.90	59.38
TCOD Treated Glass	22.39	0.09	0.52
TMPA Treated Glass	45.25	0.68	59.76

Table 2
Surface Energy (mJ/m^2) for different substrates.

Substrate	Liquid Triads		
	W-D-E	W-D-G	W-D-S
Glass	46.8 ± 0.6	64.6 ± 0.7	48.1 ± 1.3
Glass Advancing	46.4 ± 0.6	60.2 ± 0.7	40.2 ± 1.3
TCOD treated glass	22.6 ± 0.9	23.3 ± 1.2	22.6 ± 0.9
TCOD treated glass Advancing	20.8 ± 0.9	20.9 ± 1.2	20.9 ± 0.9
TMPA treated glass	46.1 ± 2.7	58.7 ± 1.1	62.9 ± 4.1
TMPA treated glass Advancing	46.3 ± 2.7	56.4 ± 1.1	61.6 ± 4.1

Impact tests were carried out under the same pressure of 2.50 psi, for comparison purposes, to keep the same velocity of impact in all the tests (with little variation). The room conditions were monitored and the air temperature was between 20 °C and 25 °C and relative air humidity between 32% and 53%. There was no control of the air temperature and air humidity. The tests were performed on the same day of the plasma cleaning and the chemical treatment to avoid contamination during storage of the materials. The velocity of impact and time of contact between the stub and backstop were recorded using the high-speed camera footage, Fig. 9 shows the impact of a stub on the backstop. The size of the beads that remained attached was measured using the ImageJ, Fig. 10 shows an example of the treated image of the disk after the impact (from Fig. 4). The interfacial energy was calculated using Eq. (7).

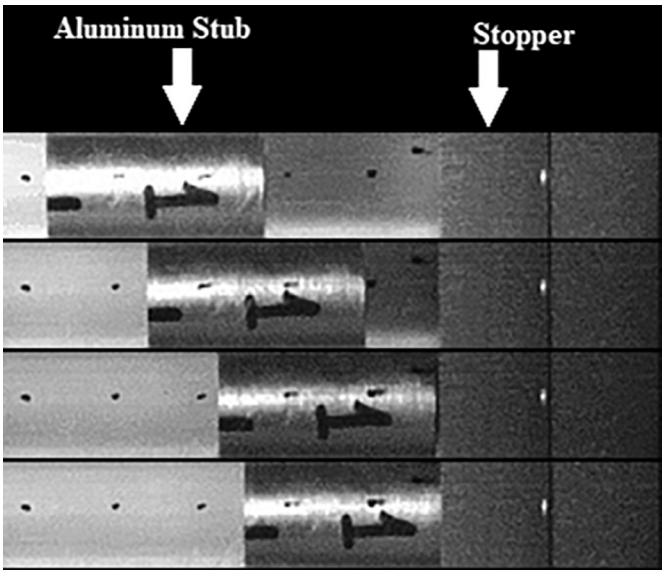

Fig. 9. Impact of Aluminum stub on stopper. Each frame recorded is 1.428 × 10^{-5} s in duration.

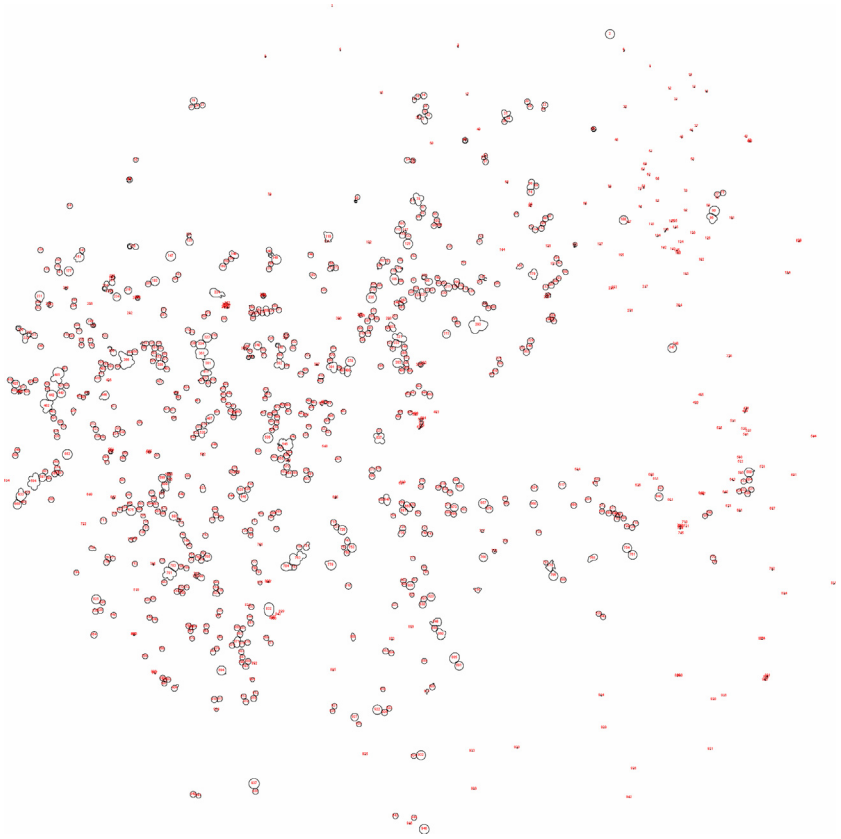

Fig. 10. Example measurement of particle size post impact using ImageJ software.

Table 3
Results of the tests with plasma cleaned beads and disks.

Trial #	Glass Disk Treatment	Bead Type Treatment	Critical Radius of Particles (m)	Mass of Particle (kg)	Impact Velocity (m/s)	Interfacial Energy (mJ/m^2)
Stub 1	Plasma	Plasma	4.48×10^{-5}	9.367×10^{-10}	1.72	46.3
Stub 2	Cleaned	Cleaned	4.35×10^{-5}	8.574×10^{-10}	1.72	43.8
Stub 3			4.63×10^{-5}	1.033×10^{-9}	1.75	50.5
Stub 5			4.78×10^{-5}	1.136×10^{-9}	1.59	48.7
Stub 7			4.20×10^{-5}	7.675×10^{-10}	1.42	33.6
Stub 8			4.66×10^{-5}	1.052×10^{-9}	1.58	46.0
Average ± one standard deviation			$4.5 \pm 0.2 \times 10^{-5}$			44.8 ± 5.9

3.1. Tests with plasma cleaned glass

These tests were carried out using glass with no chemical treatment, only with plasma cleaning to remove organic matter (contaminants) that could be present on the disk and the beads. Table 3 shows the results of the tests.

A pressure of 2.50 psi was found to give a near constant velocity with some variation noted in trials Stub 5, Stub 7 and Stub 8. Given the relatively slight variation, the causes of this variation in velocity were not investigated herein. The critical radius of the particles varied little from 42.0 μm to 47.8 μm (diameters of 84.0 and 95.6 μm, respectively). Using Eq. (7), the interfacial energy varied from 33.6 mJ/m^2, in the Stub 7 trial, to 50.5 mJ/m^2 in the Stub 3 trial. An average of 44.8 mJ/m^2 and 4.52×10^{-5} m for the interfacial energy and the critical radius of particles was recorded. The respective coefficients of variation were 13% and 4%. The average value of 44.8 mJ/m^2 is in good agreement with the literature critical surface tension value of 47 mJ/m^2 [31]. Fig. 11 shows the relationship between the impact velocity and the interfacial energy, where an unexpected behavior of slightly increasing interfacial energy with increasing impact velocity can be seen. A statistical analysis was performed and the slope is indistinguishable from zero (see *Statistical Analysis* section). Because JKR Theory assumes a smooth spherical surface, asperities and roughness on the surface of the substrate and the beads could interfere in the results, lowering the contact area and

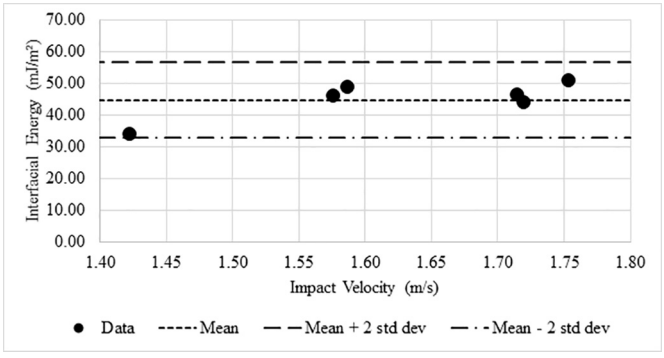

Fig. 11. Interfacial energy as a function of impact velocity.

Table 4
Results of the tests with TCOD treated beads and disks.

Trial #	Glass Disk Treatment	Bead Type Treatment	Critical Radius of Particles (m)	Mass of Particle (kg)	Impact Velocity (m/s)	Interfacial Energy (mJ/m^2)
Stub 1	TCOD	TCOD	3.09×10^{-5}	3.078×10^{-10}	1.72	26.82
Stub 2			2.49×10^{-5}	1.598×10^{-10}	1.80	17.22
Stub 5			2.66×10^{-5}	1.956×10^{-10}	1.76	20.27
Stub 12			2.53×10^{-5}	1.687×10^{-10}	1.78	21.98
Average ± one standard deviation			$2.7 \pm 0.3 \times 10^{-5}$			21.6 ± 4.0

Table 5
Results of the tests with TMPA treated beads and disks.

Trial #	Glass Disk Treatment	Bead Type Treatment	Critical Radius of Particles (m)	Mass of Particle (kg)	Impact Velocity (m/s)	Interfacial Energy (mJ/m^2)
Stub 1	TMPA	TMPA	5.11×10^{-5}	1.382×10^{-9}	1.70	47.24
Stub 6			4.94×10^{-5}	1.254×10^{-9}	1.62	35.83
Stub 9			4.16×10^{-5}	7.503×10^{-10}	1.47	41.34
Stub 12			4.15×10^{-5}	7.439×10^{-10}	1.75	35.91
Average ± one standard deviation			$4.6 \pm 0.5 \times 10^{-5}$			40.1 ± 5.4

Table 6
Comparison of surface energy measured under two different methods.

Surface Treatment	Bead Treatment	Surface Energy Contact Angles (mJ/m^2)			Interfacial Energy Adhesion Test (mJ/m^2)
		W-D-E	W-D-G	W-D-S	
Clean Glass	Clean Glass	46.4 ± 0.6	60.2 ± 0.7	40.2 ± 1.3	48.5 ± 13.3
Glass with TCOD	Glass with TCOD	20.8 ± 0.9	20.9 ± 1.2	20.9 ± 0.9	21.6 ± 4.0
Glass with TMPA	Glass with TMPA	46.3 ± 2.7	56.4 ± 1.1	61.6 ± 4.1	40.1 ± 5.4

reducing the total adhesion of the system, and thus the estimated the interfacial energy [32].

3.2. Tests with TCOD-treated glass

Similar tests were performed using TCOD to treat the glass after plasma cleaning. Table 4 shows the results of the tests. Also, working with a pressure of 2.50 psi to accelerate the stub, the velocity of the TCOD coated glass varied less than the tests with plasma cleaning only. The interfacial energy also varied less when compared with the results from the previous session, from 17.2 mJ/m^2 to 26.8 mJ/m^2, with an average of 21.6 ± 4.0 mJ/m^2. The average critical radius was 26.9 ± 3 μm (diameter of 53.8 μm). These values are smaller than the corresponding values for the plasma-cleaned glass. The results of the impact tests show the expected effect, that the hydrophobic TCOD treatment decreases the interfacial energy of the solid compared to that of plasma cleaned glass. The average value of 21.6 mJ/m^2 also agrees well with the literature value for this same type of treatment that ranges between 20 and 24 mJ/m^2 [31]. The decrease of the average critical radius is another indication that the interaction between the particles and the substrate has changed. Fig. S2, available in the supplementary material, shows that many fewer beads remained attached to the disk after the impact compared to Fig. 4. A graph (Fig. S3) similar to Fig. 11 shows the impact velocity versus interfacial energy.

3.3. Tests with TMPA treated glass

These tests were performed using TMPA to treat the glass disks and beads after plasma cleaning. Table 5 below shows the results of the tests. The same pressure of 2.50 psi was used. The average critical radius was $4.6 \pm 0.6 \times 10^{-5}$ m (diameter of 91.8 μm), similar to the critical radius of the plasma cleaned glass and greater than the critical radius of the TCOD treated glass. The interfacial energy varied from 35.8 mJ/m^2 to 47.2 mJ/m^2, with an average of 40.1 ± 5.4 mJ/m^2. Because TMPA contains amine-groups in its hydrocarbon chain, it is expected that the interfacial energy is greater than for TCOD treatment, but less than for untreated glass, because of the hydrocarbon groups in its hydrocarbon chain. The literature value of the surface tension for this chemical treatment is 37.5 mJ/m^2 [33]. The average of 40.1 mJ/m^2 is in the same order of magnitude and close to the literature value. Also, as expected, Fig. S4 shows more beads remaining after impact than TCOD treatment but fewer beads than plasma-cleaned glass treatment.

Fig. S5, available in the supplemental material, shows a different behavior the behavior observed for plasma cleaned and TCOD treatment. The interfacial energy neither increases nor decreases when the velocity increases, rather it is more likely a zero slope or a slightly negative slope, meaning the interfacial energy value is, as expected, unchanging with velocity.

3.4. Statistical analysis

To ensure that the behavior of the interfacial energy is independent of the impact velocity, statistical analysis was performed. Linear regression analysis was performed on the results of each surface treatment and the slope, intercept, and the confidence bands were determined at 95% confidence [34]. By having the slope value of zero in between the limit values it can be stated that with 95% confidence that the interfacial energy is independent of the impact velocity (slope is indistinguishable from zero), which is the expected result as the surface energy is a thermodynamic property. Figs. S6, S7 and S8 in the supplementary material show the confidence bands for the plasma cleaned, TCOD and TMPA treatment respectively.

3.5. Comparison of 'molecular surface' energy and 'mechanical' adhesion energy

Table 6 shows a comparison between the surface energy calculated from the contact angles and applying the van Oss-Good-Chaudhury method and the impact tests using the JKR theory.

Table 7
Thermodynamic work of adhesion between the glass disks and glass beads for each surface treatment.

Material	W_{adh} (mJ/m^2)
Plasma Cleaned Glass	116.20
TCOD Treated Glass	45.65
TMPA Treated Glass	116.00

With an interfacial energy of 44.8 mJ/m^2 for glass, there was a difference of 1.6 mJ/m^2 between the JKR method and the W-D-E triad from the van Oss-Good-Chaudhury method. For glass coated with TCOD, there was a difference of 0.67 mJ/m^2 between the W-D-G, W-D-S triads and the JKR method. With the TMPA treated glass, there was a difference of 6.22 mJ/m^2 between the W-D-E triad and the JKR method.

Assuming the surface energy measured in this project and the interfacial energy from the JKR method are the same entity, the values found with both methods are very similar, which suggests that both the molecular and mechanical experimental methods are valid tools for calculating surface energy. The literature values are also in good agreement with the surface energy measured with both methods.

Table 7 presents the thermodynamic work of adhesion between the glass disks and the beads (W_{adh}) in mJ/m^2 calculated using the data from Table 1, applying the Eq. (4). It was assumed that the beads and the disks with same treatment have the same LW, acid and base components.

These experimental work of adhesion values show that it is easier to adhere to plasma cleaned glass and TMPA treated glass surface than it is to TCOD treated glass, confirming what is seen in Figs. 4, S2 and S4 documenting before and after the impact test. Also, comparing the thermodynamic work of adhesion to the interfacial energy, as expected, the thermodynamic work of adhesion is about twice as large as the interfacial energy.

The data generated by the methods reported herein will next be employed in the parameter calibration of a computational model for the prediction of optimal mineral separation conditions, and the design of lab-scale equipment to determine the efficacy of mineral separations based upon adhesive forces.

4. Conclusions

An impact test apparatus (mechanical approach) and the VOGC method (molecular approach) were used to characterize the interfacial energies of a model system with a variety of surface treatments. The values measured in the experiments are in good agreement with literature values of critical surface tension. Both approaches proved to be quite comparable despite their wide variation in experimental technique. The mechanical approach is a quick and easy way to measure the total interfacial energy of two materials (particles/surface), but doescnot measure the dispersive, acidic and basic components (which are inherent for each material alone). These measurements are the first step toward development of a sustainable system that does not use water to separate and concentrate fine minerals. Future research will utilize ground minerals to determine the surface energy applying the same procedure presented here. This data will be coupled with computer simulation to predict ideal mineral separation conditions and design lab scale equipment to determine the efficacy of mineral separations based upon adhesive forces. Other applications of this research can be useful to the pharmaceutical industry, solid materials transport, and also in industries which want to avoid fine particle accumulation.

CRediT author statement

Bernardo Moreno Baqueiro Sansao: conceptualization, methodology, validation, formal analysis, investigation, data curation, writing original draft, writing review and editing **Jon Kellar:** supervision, funding acquisition, conceptualization, validation, investigation, resources, project administration, data curation, writing original draft, writing review and editing, visualization **William Cross:** supervision, funding acquisition, conceptualization, validation, investigation, resources, project administration, data curation, writing original draft, writing review and editing, visualization **Albert Romkes:** supervision, funding acquisition, conceptualization, project administration, writing review and editing **Karen Schottler:** methodology, validation, formal analysis, investigation, data curation, writing original draft

Declaration of Competing Interest

The authors declare that there is no conflict of interest.

Acknowledgments

Thanks to the National Science Foundation Grant (NSF) #1805550 Sustainable System for Mineral Beneficiation. Also, thanks to Dr. Umair Zafar for his helpful discussion and Ms. Kathryn Bozer and Mr. Bobby Santore (NSF Grants #1460912 and #1757799 (REU Site: Back to the Future)) for their generation of preliminary data.

Appendix A. Supplementary data

Supplementary data to this article can be found online at https://doi.org/10.1016/j.powtec.2021.02.029.

References

[1] B.A. Wills, T.J. Napier-Munn, Mineral Processing Technology: An Introduction to the Practical Aspects of Ore Treatment and Mineral Recovery, 2006 267–352.
[2] Donald I. Bleiwas, Estimated Water Requirements for the Conventional Flotation of Ores, 2012 USGS 2–3.
[3] J. Kolacz, Advanced sorting technologies and its potential in mineral processing, AGH J. Mining Geoeng. 36 (4) (2012) 39–48.
[4] B.C. Meikap, A.B. Daram, S. Chakraborty, S. Mohanta, Applicability of the air dense medium fluidized bed separator for cleaning of high-ash Indian thermal coals: an experimental study, South African J. Chem. Eng. 16 (1) (2011) 50–62.
[5] Ghosh, Tathagata, Modeling of an Air-Based Density Separator, Doctoral Ph.D. Dissertation submitted to the College of Engineering at the University of Kentucky, Lexington, KY, 2013.
[6] S. Mohanta, B.C. Meikap, Influence of medium particle size on the separation performance of an air dense medium fluidized bed separator for coal cleaning, J. South. Afr. Inst. Min. Metall. 115 (8) (2015) 761–766.
[7] J. He, M. Tan, R. Zhu, Z. Luo, Dry beneficiation and cleaning of Chinese high-ash coarse coal utilizing a dense-medium gas-solid fluidized bed separator, Physicochem. Problems Min. Process. (2016) 52.
[8] X. Yu, Z. Luo, H. Li, D. Gan, Beneficiation of 6-0 mm fine-grain oil shale using vibrating air-dense medium fluidized bed separator, Fuel 203 (2017) 341–351.
[9] U. Zafar, C. Hare, A. Hassanpour, M. Ghadiri, Drop test: a new method to measure the particle adhesion force, Powder Technol. 264 (2014) 236–241.
[10] G. Biresaw, C.J. Carriere, Correlation between mechanical adhesion and interfacial properties of starch/biodegradable polyester blends, J. Polym. Sci. B Polym. Phys. 39 (2001) 920–930.
[11] D.M.F. Madeira, O. Vieira, L.A. Pinheiro, B.D.M. Carvalho, Correlation between surface energy and adhesion force of polyethylene/paperboard: a predictive tool for quality control in laminated packaging, Hindawi Int. J. Chem. Eng. 2018 (2018), 2709037, , 7 pages https://doi.org/10.1155/2018/2709037.
[12] Miller, Clint Matthew, Adhesion and the Surface Energy Components of Natural Minerals and Aggregates, Master's Thesis in Geology submitted to Texas A&M University, College Station, TX, 2010.
[13] R. Tran, Z. Xu, B. Radhakrishnan, D. Winston, W. Sun, K.A. Persson, S.P. Ong, Surface energies of elemental crystals, Sci. Data 2016 (2016) 3.
[14] C. Della Volpe, S. Siboni, D. Maniglio, M. Brugnara, The solid surface free energy calculation – I. in defense of the multicomponent approach, J. Colloid Interface Sci. 271 (2) (2004) 434–453.
[15] Tserendagva, Tsend-Ayush, Characterization of Adhesion in Direct Write Ink Systems, Master's Thesis in Materials Engineering and Science submitted to South Dakota School of Mines and Technology, Rapid City, SD, 2010.
[16] Jaroslaw Drelich, Emil Chibowski, Dennis Desheng Meng, Konrad Terpilowski, Hydrophilic and Superhydrophilic surfaces and materials, Soft Matter 7 (21) (2011) 9804–9828.
[17] Jean-Charles Joud, Barthés-Labrousse, Marie-Geneviéve, Physical Chemistry and Acid-Base Properties of Surfaces, John Wiley & Sons, Inc., New Jersey, 2015.

[18] S. Siboni, C. Della Volpe, On the definition of scales in van Oss-Chaudhury-Good acid-base theory, MATCH Commun. Mathe. Comput. Chem. 56 (2) (2006).
[19] Yuehua Yuan, T. Randall Lee, Contact angle and wetting properties, Surf. Sci.Tech. 51 (2013) 3–34.
[20] K.L. Johnson, K. Kendall, A.D. Roberts, Surface energy and the contact of elastic solids, Proceed. Royal Soc. A 324 (1971) 301–313.
[21] H. Hertz, On the contact of rigid elastic solids. Miscellaneous Papers. Jones and Schott, Editors, J. reine und angewandte Mathematik 92, Macmillan, London, 1896 156.
[22] B.D. Beake, J.S.G. Ling, G.J. Leggett, Correlation of friction, adhesion, wettability and surface chemistry after argon plasma treatment of poly(ethylene terephthalate), J. Mater. Chem. 8 (1998) 2845–2854.
[23] A.J. Meuler, J.D. Smith, K.K. Varanasi, J.M. Mabry, G.H. McKinley, R.E. Cohen, Relationships between water wettability and ice adhesion, ACS Appl. Mater. Interfaces 2 (11) (2010) 3100–3110.
[24] B.D. Flinn, Improving Adhesive Bonding of Composites through Surface Characterization, https://depts.washington.edu/amtas/events/jams_08/21.Flinn.pdf 2008.
[25] I. Yildirim, Surface Free Energy Characterization of Powder. Chapter 5: Correlation between Surface Free Energy Parameters of Solids and Separation Efficiency in Mineral Beneficiation, Ph. D. Dissertation submitted to the Virginia Polytechnic Institute and State University. Blacksburg, VA, 2001.
[26] J. Taguta, B. McFadzean, C. O'Connor, The relationship between the flotation behaviour of a mineral and its surface energy properties using calorimetry, Miner. Eng. 143 (2019) 105954.
[27] C. Van Oss, M. Chaudhury, R.J. Good, Interfacial Lifshitz-van der Waals and polar interactions in macroscopic systems, Chem. Rev. 88 (6) (1988) 927–941.
[28] L.J. Robb, Introduction to Ore-Forming Processes, 2004 (United Kingdom).
[29] Si Qiu, et al., Wetting dynamics and surface energy components of single carbon fibers, J. Colloid Interface Sci. 557 (2019) 349–356.
[30] E. Chibowski, R. Perea-Carpio, Problems of contact angle and solid surface free energy determination, Adv. Colloid Interf. Sci. 98 (2) (2002) 245–264.
[31] Barry Arkles, et al., Silane Coupling Agents: Connecting Across Boundaries, Gelest, Inc, 2014 Version 3.0 pg 5.
[32] Derjaguin, Muller, Toporov, Effect of contact deformations on the adhesion of particles, J. Colloid Interface Sci. 53 (1975) 314–326.
[33] Arkles, Barry, et al., Silane Coupling Agents: Connecting Across Boundaries, Gelest, Inc, 2014 Version 3.0 pg 37.
[34] N.R. Draper, H. Smith, Applied Regression Analysis, 3rd ed. Wiley-Interscience, New York, 1998 142–146.